ACS Partner Journal

ENVIRONMENT & HEALTH

Open Access

pubs.acs.org/EnvHealth

Article

Dust Fall Microplastics from a Megacity of China Inhibit Autophagy via the PI3K/Akt/mTOR Pathway

Yajing Ma, Jinjin Yu, Jian Sun,* Yuantong Zhu, Xuan Li, Xinyao Liu, Xinya Zhang, Lingyi Liu, Lingli Li, Jiaer Yang, Weifeng Li, Kin-Fai Ho, Zhenxing Shen,* and Xiaofeng Niu*

Cite This: *Environ. Health* 2025, 3, 469−481

Read Online

ACCESS | Metrics & More | Article Recommendations | Supporting Information

ABSTRACT: The problem of microplastics (MPs) pollution has caused many health risks to residents of Chinese cities. In this study, nine kinds of MPs or microrubbers (MRs) from dust fall (DF) in Xi'an, a megacity in northwestern China, were measured by pyrolysis−gas chromatography−mass spectroscopy, namely, polyethylene, polypropylene, nylon 88, polybutylene, polytetrafluoroethylene, polyisoprene, polyvinyl chloride, natural rubber, and synthesis rubber. Here, 51.20% of MPs were extracted from the original DF (samples denoted DF-O). After the subtracting procedure, MPs and their residual (DF-S samples) were divided into two parts. Our results indicated that the DF-O and MPs samples exhibited higher cytotoxicity, inflammatory, and oxidative stress levels than the DF-S samples did. The DF-O and MPs samples suppressed autophagy by decreasing expression levels of microtubule-associated protein light chain 3 (LC3B), p-phosphatidylinositol 3-kinase (p-PI3K), phosphorylated AKT protein (p-Akt), and p-mammalian target of rapamycin (p-mTOR) while increasing the level of p62. Meanwhile, DF-O and MPs samples induced apoptosis through increasing levels of Bax/Bcl-2 and Cleaved Caspase-3/Caspase-3 in Raw264.7 cells. These trends could be reversed through removing half of the MPs in DF-O. Therefore, dust fall microplastics inhibited autophagy and induced apoptosis via activating the PI3K/Akt/mTOR pathway, increasing the Bax/Bcl-2 and Cleaved Caspase-3/Caspase-3 ratios. Here we provide a comprehensive perspective into the studies of atmospheric MPs pollution status and mechanisms of inhalation toxicity for health risk assessment of MPs in DF.

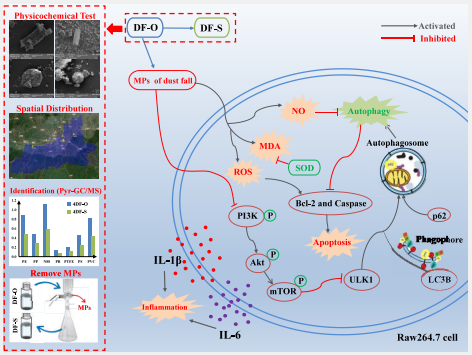

KEYWORDS: *Dust fall microplastics, Phosphatidylinositol 3-kinase/protein kinase B/mammalian target of rapamycin, Autophagy inhibition, Apoptosis, Inflammation*

■ ENVIRONMENTAL IMPLICATION

This study analyzed the components of the inhalation of dust fall microplastics (DF-MPs) from Xi'an, a megacity of northern China. Nine kinds of MPs were identified and quantified through pyrolysis gas chromatography mass spectroscopy. About half of the MPs were subtracted from DF through a water-flotation method. The results showed that changing the sizes and concentrations of MPs affected the cytotoxicity, ROS, inflammatory, autophagy, and apoptosis levels of macrophages through the PI3K/Akt/mTOR pathway and Bcl-2 and Caspase family proteins.

1. INTRODUCTION

Global annual plastic production reached 368 million metric tons in 2019, and projections indicated a 3-fold increase in this amount by 2060.[1] More than one-third of current plastic production involved production of single-use items.[2] These plastics eventually were broken down into microplastics (MPs) and nanoplastics due to physical and environmental factors such as sunlight, mechanical abrasion, and thermal oxidation.[3] Dispersed by water currents, wind, and human activities, MPs were found in marine, soil, and atmosphere samples, which threatens human health permanently and increasingly.[4] Due to being lightweight, MPs were easily suspended in the atmosphere of urban communities.[5] Various MPs accumulated on roads and other surfaces, became airborne through wind, photolysis, and decomposition, and eventually were inhaled as particulate matter.[6]

Compared to the global problem of MPs pollution, China's situation became clearly serious in past decades. Dust fall (DF) was considered as a cost-effective indicator to assess the pollution status of MPs in urban areas.[7] Research indicated that up to 30% of the compositions in the dust fall were toxic pollutants, including heavy metals, microrubbers (MRs), and MPs. In urban environments, the main types, shapes, and

Received: September 30, 2024
Revised: January 14, 2025
Accepted: January 15, 2025
Published: January 27, 2025

https://doi.org/10.1021/envhealth.4c00200
Environ. Health 2025, 3, 469−481

sources of microplastics in atmospheric dust fall were generally similar in different cities. The most abundant MPs in road dust are PE, PP, PET, and PVC.[8] The shapes of MPs in road dust have been reported as fragment, line/fiber, pellet/granule, spherule, film, paint, and foam, with average proportions of 38.5%, 25.1%, 14.7%, 12.7%, 8%, 0.9%, and 0.1%, respectively. These dust fall microplastics (DF-MPs) originated from the fragmentation of plastic debris such as clothing, car tires and municipal plastic waste.[8] There are differences in the chemical composition and pollution levels of MPs between regions. Jia et al. found that the main DF-MP types and contents of Hohhot were PEG, HTPE, PET, PPG and Nylon using nontarget and target LC-MS/MS analysis. In Shanghai, the main MP types were PET, HTPE-BD, and PEG. The main components of film microplastics in atmospheric dust fall in the Ebinur Lake Basin were PE and PP.[9] Studies showed that the microplastic levels ranging from 3.12 to 11.25 n/L in Wuliangsuhai Lake of Inner Mongolia, China were significantly higher than the 2−5 n/L range found in the rivers of Shanghai.[10]

Xi'an, as the largest city in northwestern China, is representative in terms of air pollution and has a large amount of dust fall. Therefore, Xi'an is taken as an example to study the biological toxicity and mechanism of DF-MPs in representative cities of China.

Fibrous plastics were identified in lung tissue, and finer MPs were translocated to other organs after being inhaled or ingested by humans.[11−13] Analogous research on $PM_{2.5}$ indicated that airborne pollutants were absorbed by alveoli and capillaries and led to oxidative stress and inflammation, which resulted in cell autophagy and tissue damage.[14−17] In addition, new studies indicated that MPs induced oxidative stress, inflammation, autophagy and apoptosis in macrophage cells, *Caenorhabditis elegans*, earthworms, brine shrimp, ICR mice and humans.[18−25] Moreover, small particles (<2.5 mm) are capable of crossing cell membranes and have been linked with increased risk of death from cardiovascular and respiratory diseases or lung cancer.[26−28] Although the potential risks of heavy metals in dust fall were extensively studied,[29] the impacts of microplastics in dust fall remained largely unexplored. Thus, this study aims to provide a comprehensive study on cellular toxicity, other toxicological effects, and mechanisms for DF-MPs.

Autophagy is a cellular catabolic pathway that is evolutionarily conserved from yeast to mammals.[30] It helps to degrade unfolded protein aggregates and dysfunctional organelles, and regulates cellular homeostasis.[30,31] Moreover, the protective effect of autophagy on cells prevents apoptosis, thereby improving the survival rate.[32] Further, autophagy is associated with the oxidative stress level, for example, reactive oxygen species (ROS) and malondialdehyde (MDA). As a byproduct of the antioxidative defense system, MDA could be decreased by the levels of superoxide dismutase (SOD), glutathione (GSH) and autophagy.[33] Nitric oxide (NO) induced apoptosis in human melanoma cells, and was also down-regulated by autophagy.[34] Moreover, autophagy was already demonstrated to participate in inflammation, influencing IL-6 and IL-1β and other cytokines.[35] Mechanistically, the regulation of mammalian autophagy is associated with many signaling cascades and proteins, such as the PI3K/Akt/mTOR pathway, the MAPK/mTOR pathway, the AMPK/mTOR pathway, and the Bcl-2 protein family. Among them, the PI3K/Akt/mTOR pathway is a classical autophagy signaling pathway, and also is a hotspot in cancer, lung fibrosis and immunology diseases research.[36,37] The target of rapamycin (TOR) is a highly conserved serine/threonine protein kinase that serves as a master regulator of autophagy. It integrates upstream activating signals that inhibit autophagy through the class I PtdIns3K-Akt pathway. Besides, microtubule-associated protein 1 light chain 3 beta (LC3B) and SQSTM1 (p62) are also the main protein markers in autophagy and participate in the formation of autophagosomes. Focusing on the PI3K/Akt/mTOR pathway, this study elucidates the role of autophagy in the cytotoxicity of DF-MPs. Through comparing the biological toxicity of dust fall and DF-MPs with sample removal of microplastics, we sought to understand the involvement of the PI3K/Akt/mTOR pathway in autophagy and inflammation induced by DF-MPs.[35,38,39]

Besides, apoptosis is a kind of programmed cell death, induced by high NO level, inhibiting autophagy and regulating the B-cell lymphoma-2 (Bcl-2) antiapoptotic protein, pro-apoptotic Bcl-2-associated X protein (Bax)[40] and Caspase family proteins.[41] As is well-known, Bcl-2 is known to exert antiapoptotic effects in various experimental models and apoptotic cells. Besides, it also regulates autophagy through inhibiting Parkin translocation to depolarized mitochondria in HeLa and HEK293T cells.[42] Bax is a pro-apoptotic Bcl-2 family protein that resides in the cytosol as a latent monomer until triggered to undergo a conformational change resulting in cell apoptosis. As a marker protein of apoptosis, Caspase-3 is activated and transformed into Cleaved Caspase-3. The active Caspase-3 degrades to a broad range of cellular proteins, thereby executing the final steps of apoptosis.[41] Notably, the ratio of Cleaved Caspase-3/Caspase-3 and Bax/Bcl-2 ratios determine whether a cell survives under the stimulation of apoptosis-inducing factors or not.[43] The Raw264.7 cell line was commonly used in the immunology and autophagy studies.[44] Therefore, this study used this cell line to investigate the impact of DF and DF-MPs on cell autophagy and apoptosis.

The purposes of this study were to (1) analyze the physicochemical properties of microplastics in the dust fall (with the original DF groups labeled DF-O) and those in which MPs have been removed (with these sample groups labeled DF-S); (2) evaluate the cytotoxicity induced by DF-O, DF-S and MPs; and (3) investigate the toxicological mechanism of MPs-induced autophagy and apoptosis in Raw264.7 cells.

2. MATERIALS AND METHODS

2.1. Materials and Reagents

Glass filter and mixed cellulose filter membranes (MCE membranes) were supplied by Delv Inc. (Guangdong, Foshan, China). The pyrolysis−gas chromatography−mass spectroscopy (Pyr-GC/MS) instrument was purchased from Agilent Technology (Santa Clara, CA, USA). The field-emission scanning electron microscopy (FESEM) device Sigma300 was obtained from Zeiss (Oberkochen, Germany).

The RPMI 1640 medium, phosphate buffered saline, and Annexin V-FITC/PI Apoptosis Kit were obtained from the Jiangsu KeyGEN BioTECH Corp., Ltd. (Nanjing, Jiangsu, China). The fetal bovine serum (FBS) was purchased from Gibco (Gibco-BRL, Gaithersburg, MD, USA). Enzyme-linked immunosorbent assay (ELISA) kits for rat interleukin IL-6 and IL-1β were supplied by Shanghai Xitang Biological Technology Co., Ltd. (Shanghai, China). NO, SOD, and MDA detection kits were obtained from the Jiancheng Bioengineering Institute of Nanjing (Nanjing, Jiangsu, China). All other reagents were commercially available and analytical grade.

https://doi.org/10.1021/envhealth.4c00200
Environ. Health 2025, 3, 469−481

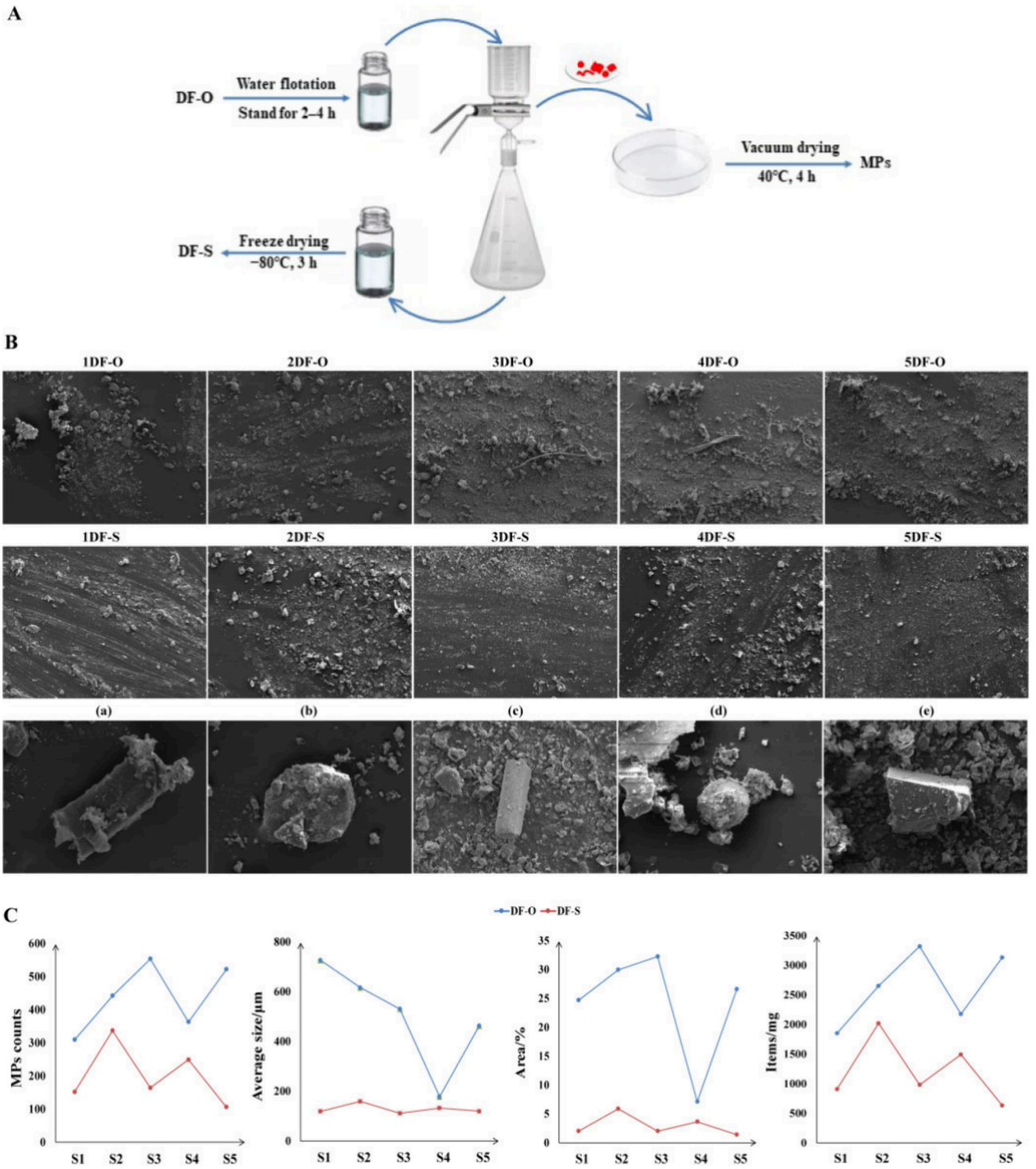

Figure 1. (A) Sample separation process of DF-S groups from five sites. (B) FE-SEM pictures in the DF-O and DF-S groups. 1DF-O: original dust falls in Site S1, 1DF-S: dust falls subtracted part of MP in Site S1; 2DF-O: original dust falls in Site S2, 2DF-S: dust falls subtracted part of MP in Site S2; 3DF-O: original dust falls in Site S3, 3DF-S: dust falls subtracted part of MP in Site S3; 4DF-O: original dust falls in Site S4, 4DF-S: dust falls subtracted part of MP in Site S4; 5DF-O: original dust falls in Site S5, 5DF-S: dust falls subtracted part of MP in Site S5. (C) Comparison between DF-O and DF-S groups in the MPs counts, average size of MPs, area ratio of MPs, and number concentrations of MPs in the site S1−S5. Site S1: Xincheng, Site S2: Beilin, Site S3: Zhouzhi, Site S4: Jingkai and Site S5: Lingtong; Different shapes of typical MP in all samples: (a) debris, (b) particle, (c) stick, (d) sphere, (e) block.

2.2. Sample Collection and Processing

2.2.1. Sample Sites. Atmospheric DF was gathered from the following five sites (Supporting Information: Figure S1) within the air monitoring system at the Xi'an Environmental Monitoring Central Station: Site S1 (34.2738°N 108.9515°E), in Xi'an Revolutionary Park in Xincheng district; Site S2 (34.2529°N 108.9728°E), at the Environment Protection Bureau of Beilin district; Site S3 (34.1599°N 108.2088°E), at the Environmental Protection Bureau of Zhouzhi district; Site S4 (34.3474°N 108.935°E), at the Administrative Commission of Jingkai district; and Site S5 (34.3748°N 109.2131°E), at the Environmental Protection Bureau of Lintong district. Samples

https://doi.org/10.1021/envhealth.4c00200
Environ. Health 2025, 3, 469−481

were collected from November 1 to 30, 2021. In 2021, the population of Xi'an city was approximately 12,873,000. This city covered an area of 10,108 km^2. The population of the Xincheng, Beilin, Zhouzhi, Jingkai, and Lintong Districts were estimated at 0.54, 0.69, 0.59, 0.55, and 0.70 million people, respectively.

2.2.2. Sampling Method. The DF-O samples were collected via dust collection tanks (bottom diam: 15 cm, height: 30 cm). The water (50 mL in the summer and 100 mL in the other seasons) and glycol were poured into the dust collection tanks to moisten the bottom and inhibit microbial growth. These tanks were putted on the roof of sampling site and placed on a platform 1.5 to 2 m meters above the ground, avoiding interference from the raise dust. These tanks were replaced at last 5 days of every month. If it rains, tanks need to be replaced in time to prevent liquid overflow.

After sampling, leaves, insects, and plant fiber were picked out from the tanks. We scraped the dust on the glass tank wall off with an iron scraper, and poured it into a breaker (500 mL). The liquid in the breaker was evaporated on a heating plate into 20 mL. The dust and water were transferred to a porcelain crucible and dried on a heating plate. The dust was dried to constant weight at 105 ± 5 °Cin a bake oven.

2.3. MPs Extraction

The main factors influencing MPs migration around the ocean, soil and air include hydrodynamics, wind power, ultraviolet radiation, and so on. In the last two decades, MPs were observed in the marine environment, freshwater.[6] These lighter MPs in the terrestrial environment are washed by surface runoff, followed by flowing into the ocean along the streams and rivers.[4] Based on this pattern, the part of MPs floating in the water had a more persistent influence on the organisms and ecosystem. Therefore, this study focused on MPs that float with water.

To obtain the MPs and DF-S parts from DF-O samples at the same time, this study used a water flotation method to separate MPs. This method did not introduce organic reagents or plastic impurity from reagent containers, avoiding potential toxicity components from reagent residue or other contaminants in the procedure of sample pretreatment. Moreover, water could reserve the soluble ingredient of the DF sample, such as metal ions, inorganic acid, salts, and so on. In addition, the water flotation method simulated the transfer process of terrestrial microplastics with rivers and rainwater in nature and, to some extent, reproduced the enrichment characteristics of microplastics in the city environment.

As shown in Figure 1A, DF samples were washed with distilled and deionized water (DDW, a resistivity of 18 MΩ·cm). Subsequently, the mixtures of water and DF were left to stand for 2−4 h, during which time the MPs rose to the supernatants. The supernatants of mixtures containing MPs were frozen at −80 °C for 3 h and subjected to freeze-drying for 48 h to obtain the MPs samples of 5 sample sites.. The resulting mixtures were referred to as the DF-S samples in this study. The DF-S mixtures were then frozen at −80 °C for 3 h and subjected to freeze-drying for 48 h. The filters and MPs attached to them were promptly transferred to glass Petri dishes and were covered with glass lids. The Petri dishes were then dried in an oven at 40 °C for approximately 4 h and stored at room temperature.

To verify the reliability of the separation method, accuracy and recovery experiments were conducted in this study. Five plastic samples were collected from five sampling sites. After cleaning and drying, these plastic samples were ground into powder and used as standard MPs samples for testing. Through this water flotation, 81.2% of the MPs can be separated from water. Due to the insufficient amount of DF for the methodology experiments, we replaced the dust fall with the road dust in this part. Three MPs standard samples (50 mg) were add into 1 g dust samples. Through this water separation, 69.5% of plastic can be isolated from the road dust samples.

2.4. Morphological Analysis by Field Emission Scanning Electron Microscopy (FESEM)

MPs pollution in the air had diverse sources. The pollution origins were primarily identified through analysis of the abundance, distribution, and characteristics of MPs, including shapes, colors, and polymer types.[45] To determine the surface characteristics of the DF-O and DF-S groups, these samples were examined using the FESEM. After the normal pretreatment, the samples were coated with a thin film of platinum and imaged using an FESEM device operated at 30 keV. Visualizations were performed at three sites on the surface of every sample.

2.5. MP Identification Methods through Pyr-GC/MS

MPs types in the urban environment mainly contained polyethylene (PE), polypropylene (PP), polyethylene terephthalate, polyisoprene (PS), polytetrafluorethylene (PTFE), polyvinyl chloride (PVC), Nylon-6.6, and the tire-wear particles natural rubber (NR), synthetic rubber (SR), and butadiene rubber (BR). These components were found in the environment and had been analyzed using the Pyr-GC/MS method.[46,47] To assess MPs contents in the DF obtained from five sites in Xi'an, all DF were subjected to Pyr-GC/MS.[48,49] Five DF-O and DF-S samples were, respectively, folded with ferromagnetic pyrofoil, loaded onto a Curie-point pyrolyzer coupled with a gas chromatography−mass spectrometry (GC/MS) system, and rapidly heated to 670 °C in 5 s. The pyrolyzed compounds were separated into a DB-5 ms capillary column. Peaks were identified based on the known fragmentation, mass spectra, and retention time for the target pyrolysis products of rubber products. Moreover, dipentene and styrene were used to quantify NR and styrene butadiene rubber (SBR), respectively. Calibration curves were established using reference standards for isoprene rubber (IR #2200; JSR Corporation) and SBR (no. 1500; JSR Corporation). As markers for butadiene rubber (e.g., vinylcyclohexene) have interference from SBR, BR is not quantified independently; instead, the sum of SBR and BR is reported to reduce uncertainties (Sun et al., 2022).

Recoveries were determined by secondary pyrolysis of the analyzed sample in the pyrofoil. No significant target fragments were observed. This proved that the pyrolysis was completed in the first run.

The limit of detection (LOD) is defined as the minimum amount of a rubber that generates the minimum distinguishable signal plus three times the standard deviation of the blank signals. No peak was detected for all target analytes in the blank calibration samples. Therefore, we approximated the mean blank signal with the calibration line intercept and the blank signal standard deviation with the standard error for the y (peak area ratio) estimate. All reference material standards for MPs were commercially available and purchased.

2.6. Quality Control (QC)

All samples were collected and pretreated by the same standardized procedure as listed in section 2.2.2. All containers used in the MPs extraction procedure are composed of glass and metal, avoiding any plastic products. These DF-O samples from 5 sites were divided to two parts, namely, DF-S and MPs, through the water flotation methods as mentioned (see section 2.3). Additionally, the biological safety of all samples is ensured through standardized irradiation sterilization procedures (X-ray irradiation for 1 h).

A good QC sample is one that is pooled from the mixture of the unknowns and has a matrix composition identical to those of the unknowns. In this study, DF-S, DF-O and MPs were detected in the same manner (see section 2.5). Moreover, data normalization algorithms were executed on the data using a software-based correction. Through these strategies, it would be relatively easy to evaluate acquired data sets for repeatability and identify any potential outliers, ensuring data effectiveness and rationality.

2.7. Culture of Raw264.7 Cells

Under the conditions of 37 °C and 5% CO_2, Raw264.7 cells were cultured in completed RPMI-1640 (containing 10% FBS and supplemented with 100 μg/mL penicillin and streptomycin). In the experiment, the cells were divided into 11 groups: the (a) control, (b) 1DF-O, (c) 2DF-O, (d) 3DF-O, (e) 4DF-O, (f) 5DF-O, (g) 1DF-S, (h) 2DF-S, (i) 3DF-S, (j) 4DF-S, and (k) 5DF-S groups, where 1DF-O was the original DF obtained at site S1, 2DF-O was DF collected from site 2, and so on. After separation, the MPs from five DF-O

https://doi.org/10.1021/envhealth.4c00200
Environ. Health 2025, 3, 469−481

samples were divided into five groups: (a) MPs-1, (b) MPs-2, (c) MPs-3, (d) MPs-4, and (e) MPs-5.

2.8. Cell Viability Assay

Raw264.7 cells were cultured at 37 °C and under 5% CO_2 for 24 h before being exposed to DF-O, DF-S and MPs. The cell viability 3-(4,5)-dimethylthiahiazo(-z-y1)-3,5-di- phenytetrazoliumromide (MTT) assay was utilized to screen concentrations of DF (50 and 100 μg/mL). Another MTT assay was used to measure cell viability at a high dose (100 μg/mL), and the culture supernatants were collected for inflammatory factor determination. The details were provided in our previous study.[33,50]

2.9. Determination of ROS and Cytokines

ROS activity was measured using a commercial ROS fluorescence probe (E004−1−1, Nanjing Jiancheng Bioengineering Institute, China) in accordance with the manufacturer's directions. Images were captured using a fluorescence microscope (Nikon DS-Ri2, Tokyo, Japan), and quantification was performed using ImageJ. The total SOD activity and NO and MDA levels were measured using commercial assay kits in accordance with the manufacturer's instruction. Commercially available ELISA kits were employed to analyze the levels of IL-6 and IL-1β in cells or cultured supernatant.

2.10. Immunology Fluorescence

Immunofluorescence was employed to investigate the impact of DF exposure on the expression levels of LC3B and p62 in Raw264.7 cells. Following the manufacturer's instruction, LC3B and p62 primary antibody (diluted to 1:500) were added and incubated overnight at 4 °C. After they were incubated with the corresponding secondary antibody at 37 °C for 50 min, stained with 4′,6-diamidino-2-phenylindole (DAPI) for 10 min, and finally sealed with neutral gum. The expression levels of the two proteins were observed under an optical microscope. ImageJ was used for quantification.

2.11. Western Blotting

The target proteins were obtained through standard procedures, as detailed in our previous article[33] and then analyzed by uisng an enhanced chemiluminescence system (Amersham Corp., CardiV, UK). ImageJ was employed for quantitative analysis. This study used the following antibodies: β-actin (ABclonal, 1:700), LC3B (Huabio, 1:15000), p62 (Huabio, 1:700), p-Akt (ABclonal, 1:700), p-PI3K (ABclonal, 1:700), p-mTOR (ABclonal, 1:4500), Bcl-2 (ABclonal, 1:700), Bax (Huabio, 1:1000), Cleaved Caspase-3 (ABclonal, 1:700) and Caspase-3 (Cohesion, 1:700). The dilution solvent for all antibodies was TBST.

2.12. Cell Flow Cytometry

Cells were seeded into a 6-well plate at a density of 1×10^5 cells per well. After administration of DF-O and DF-S and after washing off the fixative with PBS, the staining solution was added and incubated at 25 °C for 15 min. The cell suspension was detected by the flow cytometer. Flow Jo was used to analyze the data.

2.13. Statistical Analyses

All experimental data were expressed as means ± standard error of the mean (SEM). Unless otherwise specified, each experiment was performed three times (n = 3). The row data is preliminarily processed in Excel (2016) and then analyzed by GraphPad Prism 9 (GraphPad, USA). One-way ANOVA with Tukey's test was used to evaluate the statistical differences between groups and controls. A threshold of p-values <0.05 was deemed to be indicative of statistical significance, aligning with conventional standards. "#" indicates the other groups compared with the control group; "*" indicates the difference between the two groups

3. RESULTS AND DISCUSSION

3.1. Physicochemical Properties of MPs in DF-O and DF-S

The FESEM images of various samples (Figure 1B) revealed that MPs in DF-O samples had a variety of shapes including particles, flakes, blocks, and spheres. The diameters of the MPs ranged from 178.54 to 726.27 μm (Table 1). As shown in Figure 1C, MPs concentrations varied from 1854 to 3318 items/mg across sites S1−S5. Meanwhile, the average size of the MPs was 502.95 μm. It is worth noting that MPs particles in the DF-O samples larger than 500 μm constituted 75.32%, 70.05%, 67.73%, 92.87%, and 73.42% of DF-O samples from S1−S5, respectively. After water flotation, the larger MPs particles were removed, which can be seen in Figure 1B.

Table 1. MP Counts, Average Size and Abundances in Dust Fall Collected from Xi'an

Site[a]	Group	Count[b]	Size/μm[c]	Abundances (Items/mg)
S1	1DF-O	309	726.27	1854
	1DF-S	152	119.28	912
S2	2DF-O	442	616.16	2652
	2DF-S	337	159.36	2022
S3	3DF-O	553	530.69	3318
	3DF-S	164	111.30	984
S4	4DF-O	363	178.54	2178
	4DF-S	249	132.08	1494
S5	5DF-O	522	463.09	3132
	5DF-S	106	119.93	636

[a]Site S1: Xincheng, Si te S2: Beilin, Site S3: Zhouzhi, Site S4: Jingkai and Site S5: Lingtong. 1DF-O: original dust falls in Site S1, 1DF-S: dust falls subtracted part of MP in Site S1; 2DF-O: original dust falls in Site S2, 2DF-S: dust falls subtracted part of MP in Site S2; 3DF-O: original dust falls in Site S3, 3DF-S: dust falls subtracted part of MP in Site S3; 4DF-O: original dust falls in Site S4, 4DF-S: dust falls subtracted part of MP in Site S4; 5DF-O: original dust falls in Site S5, 5DF-S: dust falls subtracted part of MP in Site S5. [b]Count is the number of total plastics in the picture of one sampling locations. As shown in Figure 3, the picture is the image to one-third part of 0.5 mg sample. [c]Size is the average size of all microplastic across one sampling locations.

Pyr-GC/MS analysis revealed nine types of MPs in both the DF-O and DF-S samples in Figure 2, such as PE, PP, nylon 88 (N88), PB, PTFE, PS, PVC, NR, and SR. The concentrations of total MPs were 24.00, 118.17, 39.38, 40.32, and 41.90 μg/g for sites S1−S5, respectively (Table 2). Notably, the majority of MPs at sites S1−S5 were SR, NR, PE, N88 and PVC. SR was the most abundant, varying in concentration from 15.91 to 82.69 μg/g. The concentration scope of NR was from 6.78 to 16.10 μg/g. The PE concentration varied from 0.38 to 2.32 μg/g, with an average value of 0.98 μg/g. The N88 concentration varied from 0.25 to 1.12 μg/g, with an average value of 0.73 μg/g. The PVC concentration ranged from 0.01 to 0.81 μg/g, with an average value of 0.53 μg/g. The MPs composition in the DF varied with several factors, including geographical location, land use, traffic characteristics, and antecedent dry period.[51] Sites S1, S2, and S5 were in the residential areas of Xi'an, where the main MPs types were NR, SR, PE, PP, and N88. Sites S3 and S4 were in the center of Xi'an's industrial districts and had more industrial materials (such as PVC and PS) than the other sites did.

The significant reduction of MPs in the DF-S samples compared with DF-O groups is shown in Figure 2 and Table 1. DF-S samples contained significantly lower amounts of MPs than did DF-O (Table 1). The amounts of MPs in the 1DF-S to 5DF-S samples were 50.81%, 23.76%, 70.34%, 31.40%, and 79.69%, respectively, lower than those in samples 1DF-O to 5DF-O.

https://doi.org/10.1021/envhealth.4c00200
Environ. Health 2025, 3, 469−481

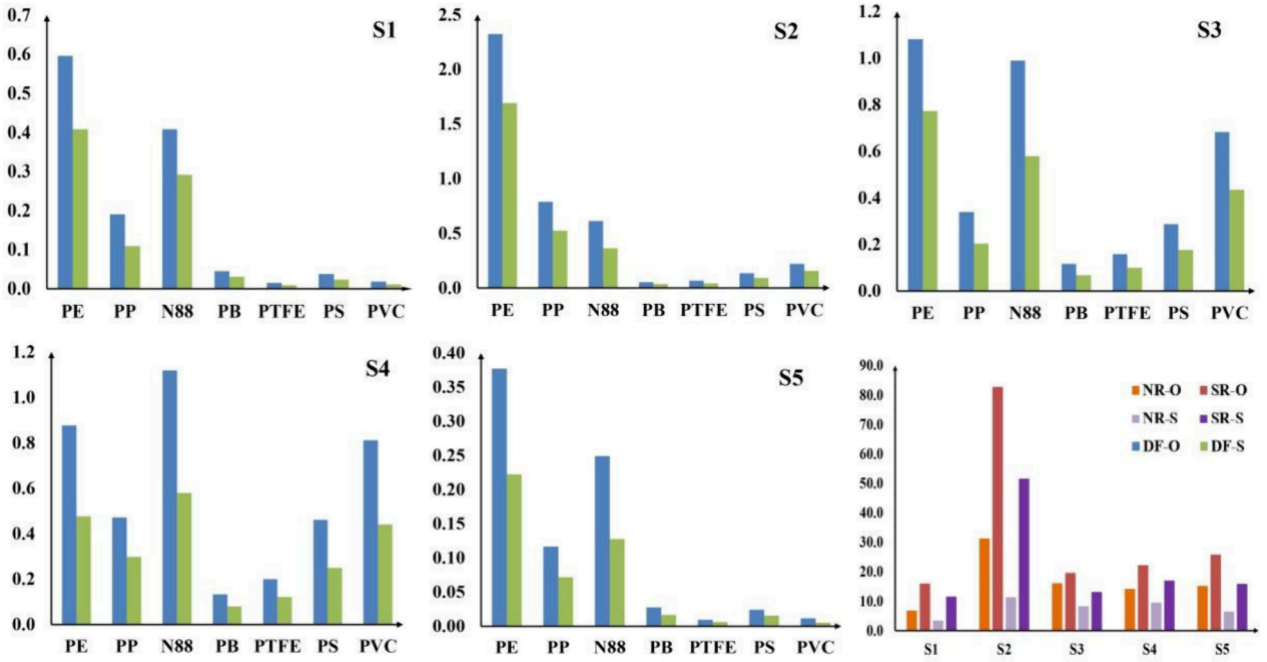

Figure 2. Content comparison of MPs, natural rubber (NR) and synthesis rubber (SR) between DF-O and DF-S groups. DF-O: original dust fall, DF-S: dust fall subtracted part of MPs. PE: polyethylene, PP: polypropylene, N88: nylon 88, PB: polybutylene, PTFE: polytetrafluorethylene, PS: polystyrene, PVC: polyvinyl chloride.

Table 2. Weight of Microplastics in the DF-O and DF-S Groups (μg/g)

		Microplastics[b]								
Site	Group[a]	PE	PP	N88	PB	PTFE	PS	PVC	NR	SR
S1	1DF-O	0.595	0.191	0.408	0.045	0.015	0.038	0.018	6.783	15.910
	1DF-S	0.408	0.109	0.291	0.030	0.009	0.024	0.011	3.422	11.540
S2	2DF-O	2.323	0.788	0.613	0.053	0.068	0.136	0.221	31.280	82.691
	2DF-S	1.692	0.524	0.363	0.035	0.042	0.093	0.156	11.340	51.525
S3	3DF-O	1.081	0.338	0.988	0.116	0.158	0.286	0.683	16.097	19.635
	3DF-S	0.773	0.202	0.578	0.067	0.099	0.176	0.434	8.193	13.169
S4	4DF-O	0.877	0.470	1.118	0.132	0.199	0.460	0.811	14.097	22.151
	4DF-S	0.477	0.296	0.579	0.079	0.121	0.249	0.441	9.533	17.024
S5	5DF-O	0.377	0.117	0.249	0.028	0.010	0.024	0.012	15.211	25.868
	5DF-S	0.223	0.072	0.128	0.017	0.006	0.016	0.005	6.421	15.810

[a]1DF-O: original dust falls in Site S1, 1DF-S: dust falls subtracted part of MP in Site S1; 2DF-O: original dust falls in Site S2, 2DF-S: dust falls subtracted part of MP in Site S2; 3DF-O: original dust falls in Site S3, 3DF-S: dust falls subtracted part of MP in Site S3; 4DF-O: original dust falls in Site S4, 4DF-S: dust falls subtracted part of MP in Site S4; 5DF-O: original dust falls in Site S5, 5DF-S: dust falls subtracted part of MP in Site S5. [b]PE: polyethylene, PP: polypropylene, N88: nylon 88, PB: polybutylene, PTFE: polytetrafluorethylene, PS: polystyrene, PVC: polyvinyl chloride, NR: natural rubber, and SR: synthesis rubber.

The diameter scope of the MPs in the DF-S samples ranged from 111.30 to 159.36 μm. Their average diameter was 128.39 μm, which was approximately a quarter of the average particle size in the DF-O samples (502.95 μm), indicating the preferential removal of larger MPs in the separation process (Table 2). Moreover, it was also noted that the average diameter of MPs in the DF-S samples reduced 83.58%, 74.13%, 79.03%, 26.02% and 74.47%, compared with DF-O samples, respectively. Most of MPs from site S4 were similar and small, indicated that the separation process did not have a major effect on this sample.

3.2. Cytotoxicity of DF-O and DF-S

As shown in Figure 3A, the MTT assay showed that cell viability values of the high dose treatment (100 μg/mL) in the DF-O groups of S1−S5 were significantly lower than those of the control group ($P < 0.05$). However, the cell viability values in the low dose group were up-regulated and had no remarkable change compared with the control group. To observe the clear comparison between DF-O and DF-S groups, the dose setting was 100 μg/mL in the following experiments in this research.

In Figure 3B, the viability data in all sites showed large gaps between DF-O and DF-S groups. DF-O and DF-S samples had lower cell viability than the control group ($P < 0.05$). More importantly, the DF-O samples in all sites showed lower cell viability than the DF-S groups clearly ($P < 0.05$). It indicated that cytotoxicity results of samples were significantly ameliorated by removing MPs partially ($P < 0.05$).

https://doi.org/10.1021/envhealth.4c00200
Environ. Health 2025, 3, 469−481

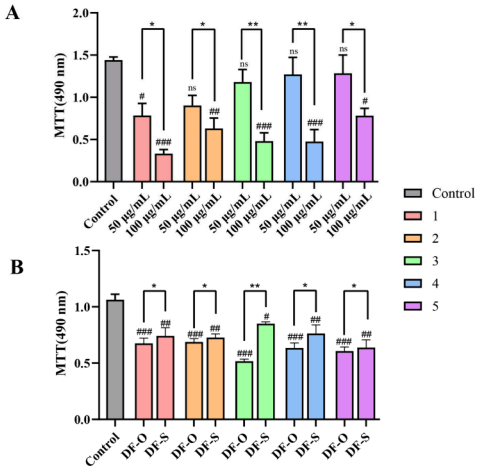

Figure 3. (A) Cell viability of DF-O in five districts of Xi'an using MTT method. (B) Cell viability of DF-O and DF-S in five districts of Xi'an using a MTT kit. DF-O: original dust fall, DF-S: dust fall subtracted part of MPs. Five distractions in Xian city, Shaanxi, China: Site S1: Xincheng, Site S2: Beilin, Site S3: Zhouzhi, Site S4: Jingkai and Site S5: Lintong. All data were presented as the mean ± SEM n = 3/group. $^{\#}P < 0.05$, $^{\#\#}P < 0.01$ and $^{\#\#\#}P < 0.001$, compared with the control group; $^{*}P < 0.05$, $^{**}P < 0.01$, DF-O vs DF-S group.

3.3. Oxidative Stress and Inflammation of DF-O, DF-S and MPs

ROS, MDA, SOD and NO were the main oxidative stress indicators and associated with autophagy. ROS and MDA levels represented cell damage and cytotoxicity, while SOD mitigated the negative impact induced by these factors. ROS served as the primary trigger for cell death.[52] After treatment with stimuli, the fluorescence intensity of cells was directly proportional to the cells' ROS levels.[50,53] As shown in Figure 4B, the ROS activity of the DF-O groups was higher than that in the control group ($P < 0.001$), while the ROS levels of DF-S group were down-regulated compared with DF-O ($P < 0.001$) in all sites. As byproduct of oxidative stress, the MDA levels in the DF-O groups of the sites S1−S4 were higher than the control group ($P < 0.05$). But the MDA levels of DF-S groups were decreased clearly compared with the DF-O groups ($P < 0.05$). Further, the SOD levels of DF-O groups decreased compared with control groups, whereas this positive indicator in the DF-S groups increased for sites S1−S5 compared to DF-O groups ($P < 0.05$).

To verify the effect on the macrophage of MPs from the dust fall, five MPs samples were treated with the Raw264.7 cells for 24h. The cell supernatants were collected to conduct MDA and SOD tests. The results showed that five MPs samples induced the higher level of MDA and lower level of SOD than control group ($P < 0.05$). These results confirmed that MPs in the dust fall induced oxidative stress in the macrophage.

Nitric oxide, a crucial signal factor within cells, is also a short-lived, highly reactive free radical. High concentrations of NO induce cell death in several types of cells. Activation of autophagy reduced the level of NO, thereby alleviating cellular damage.[15,34] As displayed in Figure 4B, DF-O samples increased NO levels compared with the control group ($P < 0.01$). In the DF-S groups, the NO levels were lower than those in the DF-O groups in all sites except S4 ($P < 0.05$), but were similar to the control group. The NO levels of MPs groups were clearly higher than those of the control group ($P < 0.01$). These results supported the hypothesis that more microplastics in the DF-O samples induced lower autophagy levels compared with DF-S samples in macrophages. That is to say, the MPs in the dust fall might inhibit autophagy to a certain degree.

IL-1β and IL-6 are important cytokines in the inflammation development process. As shown in Figure 4B, the IL-1β and IL-6 levels in the DF-O groups were obviously higher than those of control group ($P < 0.001$), which proved that these samples induced inflammation up-regulation. However, these cytokine levels of DF-S groups were down-regulated compared with DF-O samples ($P < 0.05$). Among them, the IL-1β and IL-6 levels exhibited a decreasing order of DF-O > DF-S > control group ($P < 0.05$) except for the 5DF-S sample. The IL-6, IL-1β levels of the MPs group were higher than those of the control group ($P < 0.05$). It provided strong support for the hypothesis that the microplastics in the dust fall induced intracellular inflammatory responses in Raw264.7 cells. Decreasing MPs exposure was an effective way to mitigate inflammation responses in macrophages.

3.4. Expression of LC3B and p62 Protein Detected by Immunofluorescence Assay

As the key markers of autophagy, LC3B and p62 were conserved in a catabolic process involving self-degradation of organelles and cytosolic macromolecules.[54] Generally, an increase in LC3B content and a decrease in p62 expression in liver tissue indicated the activation of autophagy flow.[55,56] This study assessed the expression of autophagy related proteins LC3B (Figure 5A, B, E) and p62 (Figure 5C, D, G). In the DF-O groups, the LC3B levels were lower, whereas the p62 levels were higher than those in the control groups ($P < 0.05$), which indicated suppression of autophagy in the DF-O groups. Notably, DF-S groups showed higher LC3B but lower p62 levels compared to those in the DF-O group ($P < 0.001$), indicating restored autophagy. The effect on autophagy of MPs extracted from dust fall were also found in the immunofluorescence assay. As shown in Figure 5E, F, the LC3B expression levels of five MPs samples were lower, but the p62 levels (Figure 5G, H) were higher than those of the control group ($P < 0.001$). These findings highlighted that microplastics in the DF-O samples led to suppression of autophagy in Raw264.7 cells.

3.5. Autophagy Protein Expression Regulated by MPs in DF in the Western Blotting Experiment

The PI3K/Akt/mTOR signal pathway was a well-established pathway in the autophagy research and also a hotspot in cancer research in recent years.[36] It can stimulate downstream effectors and mediate cell growth and survival. Abnormal activation of this pathway was a common phenomenon on malignant tumors. Through suppressing this pathway, inhibition of autophagy might effectively enhance the pro-apoptotic effect of chemotherapy.[36] Thus, the effects on this pathway of MPs in Dust fall may explain its potential risk of causing lung cancers. It was deserved in-depth research and exploration on its underlying mechanism.

As the upstream regulation cascade of autophagy, the PI3K/AKT/mTOR signaling pathway regulated the accumulation of autophagosomes in endothelial cells and human bronchial epithelial cells, resulting in fluctuation in the levels of LC3B and p62.[19] In this study, the levels of p-PI3K, p-Akt, p-mTOR, Bcl-2, and Bax proteins were examined to investigate the mechanism underlying the inhibition of autophagy and cell apoptosis (Figure 6A, B). In the DF-O groups, the levels of p-

https://doi.org/10.1021/envhealth.4c00200
Environ. Health 2025, 3, 469−481

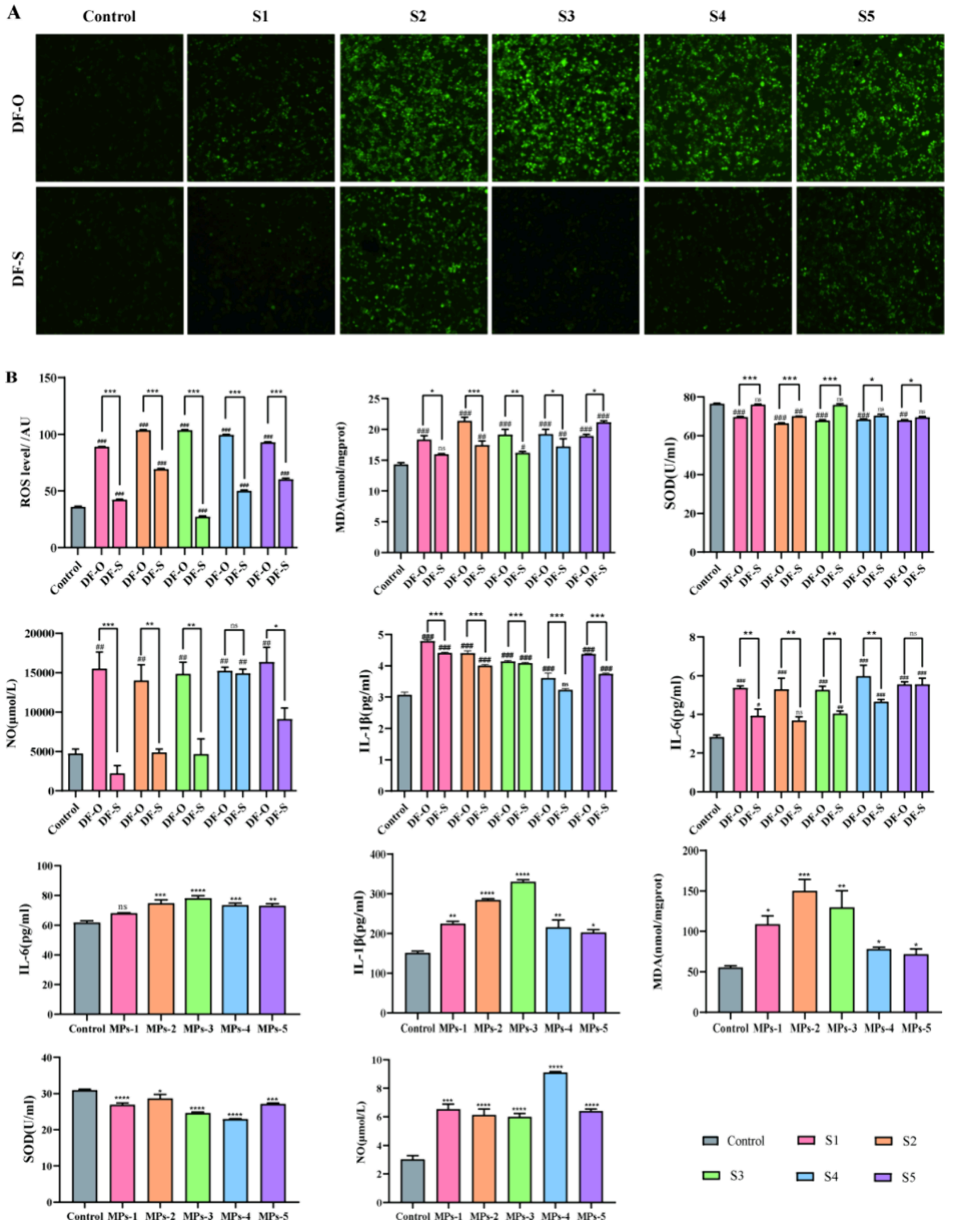

Figure 4. Oxidative stress level and inflammatory factors of DF-O, DF-S and MPs samples in five districts of Xi'an. (A) Oxidative stress level of DF-O and DF-S samples in five districts of Xi'an city (20X). (B) Expression of NO, MDA, SOD, GSH were tested by commercial reagent kits, and IL-1β and IL-6 were detected by ELISA kits. DF-O: original dust fall, DF-S: dust fall subtracted part of MPs, MPs-1: the MPs separated from 1DF-O, MPs-2: the MPs separated from 2DF-O, MPs-3: the MPs separated from 3DF-O, MPs-4: the MPs separated from 4DF-O, and MPs-5: the MPs separated from 5DF-O. Five distracts in Xian city, Shaanxi, China: Site S1: Xincheng, Site S2: Beilin, Site S3: Zhouzhi, Site S4: Jingkai and Site S5: Lintong. All data were presented as mean ± SEM $n = 3$/group. $^{\#}P < 0.05$, $^{\#\#}P < 0.01$ and $^{\#\#\#}P < 0.001$, compared with the control group; $^{*}P < 0.05$, $^{**}P < 0.01$ or $^{***}P < 0.001$, DF-O vs DF-S group.

https://doi.org/10.1021/envhealth.4c00200
Environ. Health 2025, 3, 469−481

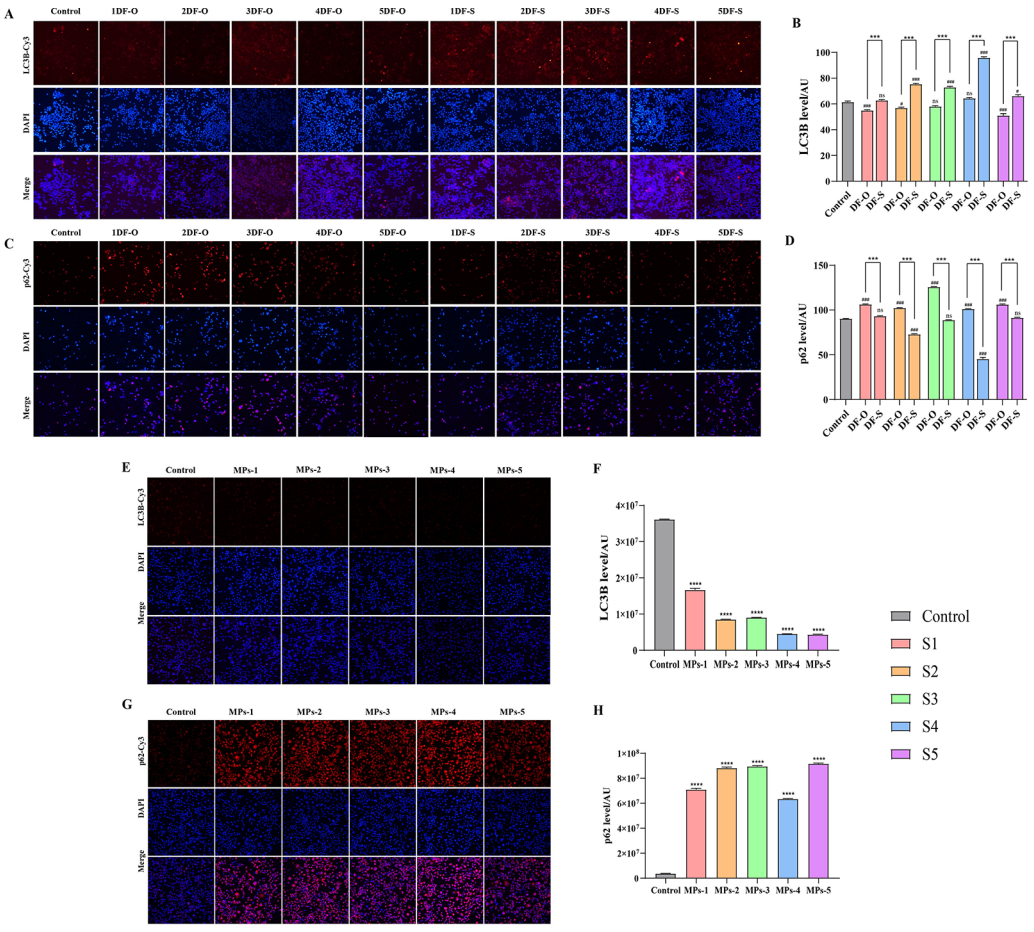

Figure 5. Immunofluorescence results of LC3B and p62 proteins. (A) Expression of LC3B protein in the DF-O and DF-S groups was detected by immunofluorescence (20 ×). (B) Immunofluorescence quantitative analysis of LC3B protein in the DF-O and DF-S groups. (C) Expression of p62 protein in the DF-O and DF-S groups was detected by immunofluorescence (20×). (D) Immunofluorescence quantitative analysis of p62 protein in the DF-O and DF-S groups. (E) Expression of LC3B protein in the MPs groups was detected by immunofluorescence (20×). (F) Immunofluorescence quantitative analysis of LC3B protein in the MPs groups. (**G**) The expression of p62 protein in the MPs groups was detected by immunofluorescence (20×). (H) Immunofluorescence quantitative analysis of p62 protein in the MPs groups. 1DF-O: original dust falls in the site S1, 1DF-S: dust falls subtracted MPs-1 in the site S1; 2DF-O: original dust falls in the site S2, 2DF-S: dust falls subtracted MPs-2 in the site S2; 3DF-O: original dust falls in the site S3, 3DF-S: dust falls subtracted MPs-3 in the site S3; 4DF-O: original dust falls in the site S4, 4DF-S: dust falls subtracted MPs-4 in the site S4; 5DF-O: original dust falls in the site S5, 5DF-S: dust falls subtracted MPs-5 in the site S5, MPs-1: the MPs separated from 1DF-O, MPs-2: the MPs separated from 2DF-O, MPs-3: the MPs separated from 3DF-O, MPs-4: the MPs separated from 4DF-O, MPs-5: the MPs separated from 5DF-O. All data were presented as mean ± SEM $n = 3$/group. $^{\#}P < 0.05$, $^{\#\#}P < 0.01$ and $^{\#\#\#}P < 0.001$, compared with the control group; $^{***}P < 0.001$, DF-O vs DF-S group.

PI3K, p-Akt, and p-mTOR were increased obviously compared with the control group ($P < 0.01$). Thus, the levels of LC3B in the DF-O groups, the autophagy marker proteins, were decreased compared with control group ($P < 0.05$), while p62 levels were increased owing to suppression of autophagy flow ($P < 0.05$). However, the p-PI3K, p-Akt, and p-mTOR expression levels of DF-S groups were lower than those of DF-O groups ($P < 0.05$). As hypothesized, the DF-S groups increased the levels of p-PI3K, p-Akt, and p-mTOR ($P < 0.05$), and the findings regarding the LC3B and p62 levels showed that autophagy flows were gained under this condition ($P < 0.01$). This clearly demonstrated that the reduction of MPs alleviated the suppression of the PI3K/Akt/mTOR-autophagy pathway and improved the autophagy level of macrophages. To ensure the autophagy inhibition activity of MPs in dust fall, this study also conducted Western blotting for MPs samples extracted from the DF-O samples. As shown in Figure 6B, MPs induced an increase of p-PI3K, p-Akt, and p-mTOR and p62 expression levels ($P < 0.01$) simultaneously, while the LC3B levels were reduced compared with the control and DF-S groups ($P < 0.01$).

3.6. Increasing Autophagy Level Decreased Apoptosis Levels in DF-S Groups

Apoptosis and autophagy play critical roles in cellular homeostasis.[57] Mild autophagy antagonizes apoptosis and protects cells from chemical injury via PI3K with an mTOR independent pathway.[58] While, autophagy-impaired cells activate apoptosis in virus-infected cells.[59] The cross-talk between apoptosis and autophagy induced by DF-MPs needs further investigation in this study. Bcl-2 and the caspase family are key apoptosis proteins, jointly determining the apoptosis process. Bax is a pro-apoptotic protein that plays a pivotal role in controlling apoptosis.[60] Bcl-2 promotes cell survival and regulates mitochondrial dynamics like fusion and fission. It also inhibits apoptosis via blocking the activation of caspases.[61] Therefore, Bax/Bcl-2 and Cleaved Caspase-3/Caspase-3 ratios reflected the level of cell apoptosis. As shown in Figure 6, these

https://doi.org/10.1021/envhealth.4c00200
Environ. Health 2025, 3, 469−481

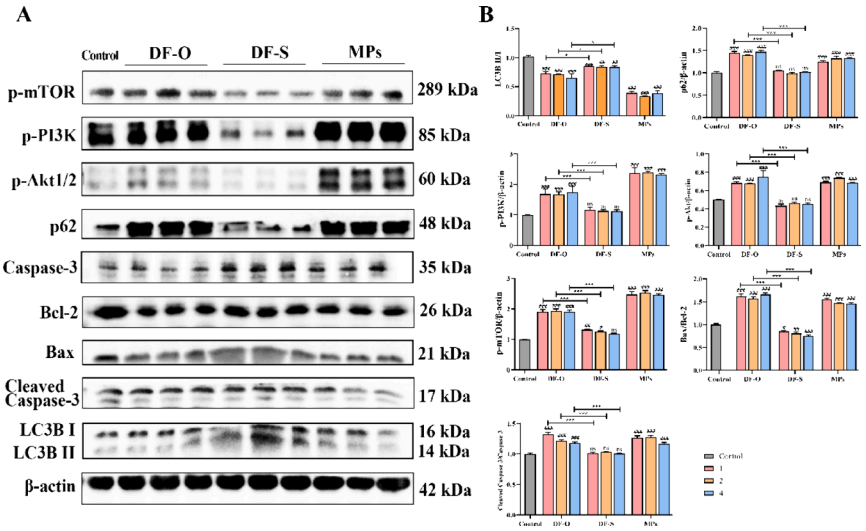

Figure 6. Protein levels of PI3K/Akt/mTOR signaling pathway in DF-O and DF-S samples. (A) Expression of β-actin, LC3B, p62, p-PI3K, p-Akt, p-mTOR Bcl-2, Bax, Caspase-3 and Cleaved Caspase-3 was detected by Western blot. (B) Quantitative analysis of LC3B, p62, p-PI3K, p-Akt, p-mTOR Bcl-2, Bax, Caspase-3 and Cleaved Caspase-3 proteins from ten groups. Quantification of the relative expression of LC3B II/I, p62/β-actin, p-PI3K/β-actin, p-Akt/β-actin, p-mTOR/β-actin, Bax/Bcl-2 and Cleaved Caspase-3/Caspase-3 was performed by densitometric analysis. The data are presented as mean ± SEM n = 3/group. $^{\#}P < 0.05$, $^{\#\#}P < 0.01$ and $^{\#\#\#}P < 0.001$, compared with the control group; $^{*}P < 0.05$, $^{**}P < 0.01$ or $^{***}P < 0.001$, vs DF-O group. DF-O: original dust fall, DF-S: dust fall subtracted part of MPs, MPs-1: the MPs separated from 1DF-O, MPs-2: the MPs separated from 2DF-O, MPs-3: the MPs separated from 3DF-O, MPs-4: the MPs separated from 4DF-O, MPs-5: the MPs separated from 5DF-O. Three districts in Xian city, Shaanxi, China, S1: Xincheng, S2: Beilin, S4: Jingkai.

two ratios of DF-O group and MPs groups were evidently higher than the control group ($P < 0.05$), which proved that DF-O and MPs enhanced the apoptosis. These ratios of the DF-S groups decreased compared with the DF-O groups ($P < 0.001$).

Further, the apoptosis enhancement originated from autophagy suppression through activation of apoptosis-associated caspase.[41,62] Due to removal of MPs from DF-O, the DF-S group reduced the autophagy inhibition effect according to above-mentioned results. The cell flow cytometry results (Supporting Information: Figure S2) showed, apoptosis level of DF-O group is higher than the control group ($P < 0.01$). While, the cell apoptosis rate of the DF-S group declined clearly compared to DF-O group ($P < 0.05$). Consisted with viewpoint of the references, the apoptosis level decreased significantly after lessening the autophagy inhibition.

This evidence indicated that cell apoptosis of DF-O and MPs groups was activated through inhibiting protective autophagy of the Raw264.7 cell. Thus, we speculated that reducing MPs was beneficial to diminish cytotoxicity of DF samples through activating autophagy and further reducing apoptosis.

3.7. Potential Molecular Mechanism of DF-MPs Suppressing Autophagy

The ROS levels were up-regulated in the DF-O and MPs groups, which induced lipid peroxidation and protein denaturation and thereby exerted obvious toxic effects on cells. Generally, ROS was produced by mitochondria, while it generated energy. When mitochondria cannot obtain enough O_2 to accept electrons in oxidative phosphorylation, the uncoupled free electrons increase and generate ROS in the cell.[63] With ROS accumulation, the permeability of the mitochondrial membrane increases, and the ROS can be released into the cytoplasm and induce peripheral mitochondria to react, resulting in imbalance of intracellular redox metabolism and ultimately extensive mitochondrial damage.

As a part of cell autophagy, mitophagy plays an important role in cell homeostasis by degrading and removing damaged mitochondria.[64] The phosphatase and tension homologue deleted on chromosome 10-induced kinase 1 (PINK1)/Parkin signaling pathway plays a key role in mitophagy.[65] PINK1 shuttles between the cytosol and the mitochondria. It can interact with Parkin, a ubiquitin E3 ligase encoded by the Park2 gene. Under normal conditions, PINK1 was degraded by presenilin-associated rhomboid-like protease (PARL). However, the activity of PARL was inhibited after mitochondrial membrane potential dissipation. The excessive PINK1 was recruited to the mitochondria membrane and then promoted Parkin phosphorylation. Polyubiquitinated proteins in the mitochondrial outer membrane trigger the migration of Ub and LC3 binding adaptor protein p62.[64] These molecule links formed the fusion of mitophagosomes and lysosomes, mediating the degradation of the damaged mitochondria. When mitophagy was blocked by autophagy inhibitors, air pollutants and MPs, the damaged mitochondria cannot be degraded and release excessive ROS into the cell, subsequently leading to cell apoptosis, death[66] and tissue damage.[67] The underlying molecular mechanism of DF-MPs on mitophagy and autophagy is studied in another program of our team.

To sum up, the MPs in the DF-O groups activated the PI3K/Akt/mTOR pathway, which further inhibited the autophagy flow of macrophages, ultimately causing inflammatory response, oxidative stress, and even cell apoptosis. Understanding the effects of the PI3K/Akt/mTOR pathway could provide valuable information for screening drugs that inhibit the toxicity of MPs and prevent lung diseases such as pneumonia and lung cancer.

https://doi.org/10.1021/envhealth.4c00200
Environ. Health 2025, 3, 469−481

4. CONCLUSIONS

This study compared DF in a megacity of China to assess the impact of MPs on cell viability, oxidative stress response and inflammation levels. The results indicated that MPs resulted in suppression of autophagy and triggered higher cytotoxicity, inflammation and ROS, leading to cell apoptosis. On this basis, immunofluorescence and Western blotting results further revealed that MPs significantly inhibited autophagy by inhibiting the PI3K/Akt/mTOR signaling pathway, and increased cell apoptosis through upregulating the levels of Bax/Bcl-2 and Cleaved Caspase-3/Caspase-3. Note that limitations such as incomplete removal of MPs and sampling in a single city were present. In future research, more efficient strategies of separating MPs from air pollutants will be further explored and optimized. Regarding the verification of universality of our results, more DF from the representative cities of China should be collected for the next study. Nevertheless, the crucial findings of this study demonstrated the necessity in scientific governance of atmospheric MPs. More importantly, this research could provide potential targets for drug research and development (R&D) against the health risks associated with MPs exposure in the present and future human life.

■ ASSOCIATED CONTENT

Supporting Information

The Supporting Information is available free of charge at https://pubs.acs.org/doi/10.1021/envhealth.4c00200.

Detailed locations of five samples collection sites of Xi'an city in China; apoptosis rate of DF-O and DF-S groups (PDF)

■ AUTHOR INFORMATION

Corresponding Authors

Xiaofeng Niu − *School of Pharmacy, Xi'an Jiaotong University, Xi'an 710061, China;* orcid.org/0000-0001-8851-5938; Email: niuxf@mail.xjtu.edu.cn

Zhenxing Shen − *Department of Environmental Sciences and Engineering, Xi'an Jiaotong University, Xi'an 710049, China;* orcid.org/0000-0002-1294-1751; Email: zxshen@mail.xjtu.edu.cn

Jian Sun − *Department of Environmental Sciences and Engineering, Xi'an Jiaotong University, Xi'an 710049, China;* Email: sunjian0306@mail.xjtu.edu.cn

Authors

Yajing Ma − *School of Pharmacy, Xi'an Jiaotong University, Xi'an 710061, China;* orcid.org/0009-0000-0048-6811

Jinjin Yu − *School of Pharmacy, Xi'an Jiaotong University, Xi'an 710061, China*

Yuantong Zhu − *China Energy Engineering Group Shaanxi Electric Power Design Institute Co., Ltd., Xi'an 710054, China*

Xuan Li − *Xi'an Ecology and Environment Bureau, Xi'an Environmental Monitoring Station, Xi'an 710054, China*

Xinyao Liu − *School of Pharmacy, Xi'an Jiaotong University, Xi'an 710061, China*

Xinya Zhang − *School of Pharmacy, Xi'an Jiaotong University, Xi'an 710061, China*

Lingyi Liu − *School of Pharmacy, Xi'an Jiaotong University, Xi'an 710061, China*

Lingli Li − *School of Pharmacy, Xi'an Jiaotong University, Xi'an 710061, China*

Jiaer Yang − *Department of Environmental Sciences and Engineering, Xi'an Jiaotong University, Xi'an 710049, China*

Weifeng Li − *School of Pharmacy, Xi'an Jiaotong University, Xi'an 710061, China*

Kin-Fai Ho − *The Jockey Club School of Public Health and Primary Care, The Chinese University of Hong Kong, Hong Kong 999077, Hong Kong, China;* orcid.org/0000-0001-7464-3437

Complete contact information is available at: https://pubs.acs.org/10.1021/envhealth.4c00200

Notes

The authors declare no competing financial interest.

■ ACKNOWLEDGMENTS

This work was supported by the Natural Science Foundation of Shaanxi Province, China (2024JC-ZDXM-20); and Xi'an Jiaotong University Interdisciplinary Training Program (IDT2220).

■ ABBREVIATIONS

MPs, microplastics; MRs, microrubbers; DF, dust fall; DF-O, original DF; LC3, microtubule-associated protein light chain 3; p-PI3K, p-phosphatidylinositol 3-kinase; p-Akt, phosphorylated AKT protein; p-mTOR, p-mammalian target of rapamycin; DF-MPs, dust fall microplastics; ROS, reactive oxygen species; MDA, malondialdehyde; SOD, superoxide dismutase; GSH, glutathione; NO, nitric oxide; TOR, target of rapamycin; p62, SQSTM1; Bcl-2, B-cell lymphoma-2; DDW, distilled and deionized water; FESEM, field emission scanning electron microscope; Pyr-GC/MS, pyrolysis−gas chromatography−mass spectroscopy; PE, polyethylene; PP, polypropylene; PS, polyisoprene; PTFE, polytetrafluorethylene; PVC, polyvinyl chloride; NR, natural rubber; SR, synthetic rubber; GC/MS, gas chromatography−mass spectrometry; LOD, limit of detection; QC, quality control; MTT, 3-(4,5-dimethylthiazol-2-yl)-2,5-diphenytetrazolium bromide; DAPI, 4′,6-diamidino-2-phenylindole; SEM, standard error of the mean

■ REFERENCES

(1) Evangeliou, N.; Tichý, O.; Eckhardt, S.; Zwaaftink, C. G.; Brahney, J. Sources and fate of atmospheric microplastics revealed from inverse and dispersion modelling: From global emissions to deposition. *J. Hazard Mater.* **2022**, *432*, 128585.

(2) Landrigan, P. J.; Raps, H.; Cropper, M.; Bald, C.; Brunner, M.; Canonizado, E. M.; et al. The Minderoo-Monaco Commission on Plastics and Human Health. *Ann. Glob Health* **2023**, *89* (1), 1−215.

(3) Zhao, X.; Wang, J.; Yee Leung, K. M.; Wu, F. Color: An Important but Overlooked Factor for Plastic Photoaging and Microplastic Formation. *Environ. Sci. Technol.* **2022**, *56* (13), 9161−9163.

(4) Huang, D.; Tao, J.; Cheng, M.; Deng, R.; Chen, S.; Yin, L.; et al. Microplastics and nanoplastics in the environment: Macroscopic transport and effects on creatures. *J. Hazard Mater.* **2021**, *407*, 124399.

(5) Khodabakhshloo, N.; Abbasi, S.; Turner, A. Resuspension of microplastics and microrubbers in a semi-arid urban environment (Shiraz, Iran). *Environ. Pollut.* **2023**, *316*, 120575.

(6) Abbasi, S.; Keshavarzi, B.; Moore, F.; Turner, A.; Kelly, F. J.; Dominguez, A. O.; et al. Distribution and potential health impacts of microplastics and microrubbers in air and street dusts from Asaluyeh County, Iran. *Environ. Pollut.* **2019**, *244*, 153−164.

(7) Su, L.; Nan, B.; Craig, N. J.; Pettigrove, V. Temporal and spatial variations of microplastics in roadside dust from rural and urban Victoria, Australia: Implications for diffuse pollution. *Chemosphere* **2020**, *252*, 126567.
(8) Yang, C.; Niu, S.; Xia, Y.; Wu, J. Microplastics in urban road dust: Sampling, analysis, characterization, pollution level, and influencing factors. *TrAC Trends in Analytical Chemistry* **2023**, *168*, 117348.
(9) Zhang, Z.; Zulpiya, M.; Wang, P. Occurrence and sources of microplastics in dust of the Ebinur lake Basin, northwest China. *Environmental Geochemistry and Health* **2023**, *45* (5), 1461−1474.
(10) Jia, B.; Zhu, K.; Bai, Z.; Abudula, A.; Liu, B.; Yan, J. Non targeted and targeted LC-MS/MS insights into the composition and concentration of atmospheric microplastics and additives: Impacts and regional changes of sandstorms in Shanghai and Hohhot, China. *Sci. Total Environ.* **2024**, *953*, 176254.
(11) Pauly, J. L.; Stegmeier, S. J.; Allaart, H. A.; Cheney, R. T.; Zhang, P. J.; Mayer, A. G.; Streck, R. J. Inhaled cellulisic and plastic fibers found in human lung tissue. *Cancer Epidemiol. Biomark. Prev* **1998**, *7* (5), 419.
(12) Lett, Z.; Hall, A.; Skidmore, S.; Alves, N. J. Environmental microplastic and nanoplastic: Exposure routes and effects on coagulation and the cardiovascular system. *Environ. Pollut.* **2021**, *291*, 118190.
(13) O'Brien, S.; Okoffo, E. D.; Rauert, C.; O'Brien, J. W.; Ribeiro, F.; Burrows, S. D.; et al. Quantification of selected microplastics in Australian urban road dust. *J. Hazard Mater.* **2021**, *416*, 125811.
(14) Salimi, A.; Alavehzadeh, A.; Ramezani, M.; Pourahmad, J. Differences in sensitivity of human lymphocytes and fish lymphocytes to polyvinyl chloride microplastic toxicity. *Toxicol Ind. Health* **2022**, *38* (2), 100−111.
(15) Li, W.; Li, W.; Yu, J.; Liu, F.; Zang, L.; Xiao, X.; et al. Fraxin inhibits lipopolysaccharide-induced inflammatory cytokines and protects against endotoxic shock in mice. *Fundam Clin Pharmacol* **2020**, *34* (1), 91−101.
(16) Li, W.; Zhi, W.; Liu, F.; Zhao, J.; Yao, Q.; Niu, X. Paeoniflorin inhibits VSMCs proliferation and migration by arresting cell cycle and activating HO-1 through MAPKs and NF-κB pathway. *Int. Immunopharmacol* **2018**, *54*, 103−111.
(17) Li, W.; Yu, J.; Xiao, X.; Zang, L.; Yang, Y.; Yu, J.; et al. Imperatorin reduces the inflammatory response of atherosclerosis by regulating MAPKs signaling pathway in vivo and in vitro. *Int. Immunopharmacol* **2021**, *90*, 107170.
(18) Chen, W.; Chu, Q.; Ye, X.; Sun, Y.; Liu, Y.; Jia, R.; et al. Canidin-3-glucoside prevents nano-plastics induced toxicity via activating autophagy and promoting discharge. *Environ. Pollut.* **2021**, *274*, 116524.
(19) Dikic, I.; Elazar, Z. Mechanism and medical implications of mammalian autophagy. *Nat. Rev. Mol. Cell Biol.* **2018**, *19* (6), 349−364.
(20) Halle, L. L.; Palmqvist, A.; Kampmann, K.; Khan, F. R. Ecotoxicology of micronized tire rubber: Past, present and future considerations. *Sci. Total Environ.* **2020**, *706*, 135694.
(21) Chen, J.; Xu, Z.; Liu, Y.; Mei, A.; Wang, X.; Shi, Q. Cellular absorption of polystyrene nanoplastics with different surface functionalization and the toxicity to RAW264.7 macrophage cells. *Ecotoxicol Environ. Saf* **2023**, *252*, 114574.
(22) Lee, S.; Kang, K.-K.; Sung, S.-E.; Choi, J.-H.; Sung, M.; Seong, K.-Y. In Vivo Toxicity and Pharmacokinetics of Polytetrafluoroethylene Microplastics in ICR Mice. *Polymers* **2022**, *14* (11), 2220.
(23) Li, Y.; Tao, L.; Wang, Q.; Wang, F.; Li, G.; Song, M. Potential Health Impact of Microplastics: A Review of Environmental Distribution, Human Exposure, and Toxic Effects. *Environment & Health* **2023**, *1* (4), 249−257.
(24) Suman, T. Y.; Jia, P.-P.; Li, W.-G.; Junaid, M.; Xin, G.-Y.; Wang, Y. Acute and chronic effects of polystyrene microplastics on brine shrimp: First evidence highlighting the molecular mechanism through transcriptome analysis. *J. Hazard Mater.* **2020**, *400*, 123220.
(25) Bao, X.; Wang, Z.; Liu, L.; Wang, D.; Gu, Y.; Chen, L. The combined effects of azoxystrobin and different aged polyethylene microplastics on earthworms (Eisenia fetida): A systematic evaluation based on oxidative damage and intestinal function. *Sci. Total Environ.* **2024**, *923*, 171494.
(26) Vethaak, A. D.; Legler, J. Microplastics and human health. *Science* **2021**, *371* (6530), 672−674.
(27) Liu, Z.; You, X.-y. Recent progress of microplastic toxicity on human exposure base on in vitro and in vivo studies. *Sci. Total Environ.* **2023**, *903*, 166766.
(28) Mittal, N.; Tiwari, N.; Singh, D.; Tripathi, P.; Sharma, S. Toxicological impacts of microplastics on human health: a bibliometric analysis. *Environmental Science and Pollution Research* **2024**, *31* (46), 57417−57429.
(29) Gunawardana, C.; Goonetilleke, A.; Egodawatta, P.; Dawes, L.; Kokot, S. Source characterisation of road dust based on chemical and mineralogical composition. *Chemosphere* **2012**, *87* (2), 163−170.
(30) Yang, Z.; Klionsky, D. J. Mammalian autophagy: core molecular machinery and signaling regulation. *Curr. Opin Cell Biol.* **2010**, *22* (2), 124−131.
(31) Cao, J.; Hou, S.; Chen, Z.; Yan, J.; Chao, L.; Qian, Y.; et al. Interleukin-37 relieves PM2.5-triggered lung injury by inhibiting autophagy through the AKT/mTOR signaling pathway in vivo and in vitro. *Ecotoxicol Environ. Saf* **2024**, *269*, 115816.
(32) Wu, H.; Li, W.; Wang, T.; Rong, Y.; He, Z.; Huang, S. α-Tomatine, a novel early-stage autophagy inhibitor, inhibits autophagy to enhance apoptosis via Beclin-1 in Skov3 cells. *Fitoterapia* **2021**, *152*, 104911.
(33) Sun, J.; Shen, Z.; Niu, X.; Zhang, Y.; Zhang, B.; Zhang, T.; et al. Cytotoxicity and Potential Pathway to Vascular Smooth Muscle Cells Induced by PM2.5 Emitted from Raw Coal Chunks and Clean Coal Combustion. *Environ. Sci. Technol.* **2020**, *54* (22), 14482−14493.
(34) He, H.; Feng, Y. S.; Zang, L. H.; Liu, W. W.; Ding, L. Q.; Chen, L. X.; et al. Nitric oxide induces apoptosis and autophagy; autophagy down-regulates NO synthesis in physalin A-treated A375-S2 human melanoma cells. *Food Chem. Toxicol.* **2014**, *71*, 128−135.
(35) Jin, L.; Li, J.; Yang, S.; Zhang, R.; Hu, C.; Chen, Y.; et al. MAPK p38/Ulk1 pathway inhibits autophagy and induces IL-1β expression in hepatic stellate cells. *Am. J. Physiol Gastrointest Liver Physiol* **2022**, *322* (3), G360−G367.
(36) Chen, S.; Yao, L. Autophagy inhibitor potentiates the antitumor efficacy of apatinib in uterine sarcoma by stimulating PI3K/Akt/mTOR pathway. *Cancer Chemother Pharmacol* **2021**, *88* (2), 323−334.
(37) Cong, L. H.; Li, T.; Wang, H.; Wu, Y. N.; Wang, S. P.; Zhao, Y. Y.; et al. IL-17A-producing T cells exacerbate fine particulate matter-induced lung inflammation and fibrosis by inhibiting PI3K/Akt/mTOR-mediated autophagy. *J. Cell Mol. Med.* **2020**, *24* (15), 8532−8544.
(38) He, J.; Peng, H.; Wang, M.; Liu, Y.; Guo, X.; Wang, B.; et al. Isoliquiritigenin inhibits TGF-β1-induced fibrogenesis through activating autophagy via PI3K/AKT/mTOR pathway in MRC-5 cells. *Acta Biochimica et Biophysica Sinica* **2020**, *52* (8), 810−820.
(39) Wang, H; Zhang, S.; Qian, W.; Ma, J. The role of autophagy in pulmonary fibrosis and research progress in traditional Chinese medicine treatment. *Modern Journal of Integrated Traditional Chinese and Western Medicine* **2023**, *31* (14), 2023−2028.
(40) McHenry, M. W.; Shi, P.; Camara, C. M.; Cohen, D. T.; Rettenmaier, T. J.; Adhikary, U.; et al. Covalent inhibition of pro-apoptotic BAX. *Nat. Chem. Biol.* **2024**, *23* (6), 1537−1543.
(41) Li, M.; Tan, J.; Miao, Y.; Lei, P.; Zhang, Q. The dual role of autophagy under hypoxia-involvement of interaction between autophagy and apoptosis. *Apoptosis* **2015**, *20* (6), 769−777.
(42) Zhang, Z.; Chen, Z.; Liu, R.; Liang, Q.; Peng, Z.; Yin, S.; et al. Bcl-2 Proteins Regulate Mitophagy in Lipopolysaccharide-Induced Acute Lung Injury via PINK1/Parkin Signaling Pathway. *Oxid Med. Cell Longev* **2020**, *2020*, 1−20.
(43) Yu, H. H.; Qiu, Y. X.; Li, B.; Peng, C. Y.; Zeng, R.; Wang, W. Kadsura heteroclita stem ethanol extract protects against carbon

tetrachloride-induced liver injury in mice via suppression of oxidative stress, inflammation, and apoptosis. *J. Ethnopharmacol* **2021**, *267*, 113496.
(44) Ma, Y.; He, Y.; Yin, T.; Chen, H.; Gao, S.; Hu, M. Metabolism of Phenolic Compounds in LPS-stimulated Raw264.7 Cells Can Impact Their Anti-inflammatory efficacy: Indication of Hesperetin. *J. Agric. Food Chem.* **2018**, *66* (24), 6042−6052.
(45) Pan, Z.; Sun, Y.; Liu, Q.; Lin, C.; Sun, X.; He, Q.; et al. Riverine microplastic pollution matters: A case study in the Zhangjiang River of Southeastern China. *Mar. Pollut. Bull.* **2020**, *159*, 111516.
(46) Fan, W.; Salmond, J. A.; Dirks, K. N.; Cabedo Sanz, P.; Miskelly, G. M.; Rindelaub, J. D. Evidence and Mass Quantification of Atmospheric Microplastics in a Coastal New Zealand City. *Environ. Sci. Technol.* **2022**, *56* (24), 17556−17568.
(47) Fischer, M.; Scholz-Böttcher, B. M. Simultaneous Trace Identification and Quantification of Common Types of Microplastics in Environmental Samples by Pyrolysis-Gas Chromatography-Mass Spectrometry. *Environ. Sci. Technol.* **2017**, *51* (9), 5052−5060.
(48) Sun, J.; Ho, S. S. H.; Niu, X.; Xu, H.; Qu, L.; Shen, Z.; et al. Explorations of tire and road wear microplastics in road dust PM2.5 at eight megacities in China. *Sci. Total Environ.* **2022**, *823*, 153717.
(49) Liu, M.; Xu, H.; Feng, R.; Gu, Y.; Bai, Y.; Zhang, N.; et al. Chemical composition and potential health risks of tire and road wear microplastics from light-duty vehicles in an urban tunnel in China. *Environ. Pollut.* **2023**, *330*, 121835.
(50) Sun, J.; Yu, J.; Niu, X.; Zhang, X.; Zhou, L.; Liu, X.; et al. Solid fuel derived PM2.5 induced oxidative stress and according cytotoxicity in A549 cells: The evidence and potential neutralization by green tea. *Environ. Int.* **2023**, *171*, 107674.
(51) Zhou, Q.; Tian, C.; Luo, Y. Various forms and deposition fluxes of microplastics identified in the coastal urban atmosphere. *Chin. Sci. Bull.* **2017**, *62* (33), 3902−3909.
(52) Villalpando-Rodriguez, G. E.; Gibson, S. B. Reactive Oxygen Species (ROS) Regulates Different Types of Cell Death by Acting as a Rheostat. *Oxid Med. Cell Longev* **2021**, *2021*, 1−17.
(53) Sun, J.; Shen, Z.; Zeng, Y.; Niu, X.; Wang, J.; Cao, J.; et al. Characterization and cytotoxicity of PAHs in PM2.5 emitted from residential solid fuel burning in the Guanzhong Plain, China. *Environ. Pollut.* **2018**, *241*, 359−368.
(54) Wu, S.; Lu, H.; Wang, W.; Song, L.; Liu, M.; Cao, Y.; et al. Prevention of D-GalN/LPS-induced ALI by 18β-glycyrrhetinic acid through PXR-mediated inhibition of autophagy degradation. *Cell Death Dis* **2021**, *12* (5), 480−493.
(55) Hu, C.; Zhao, L.; Shen, M.; Wu, Z.; Li, L. Autophagy regulation is an effective strategy to improve the prognosis of chemically induced acute liver injury based on experimental studies. *J. Cell Mol. Med.* **2020**, *24* (15), 8315−8325.
(56) Shi, H.; Han, W.; Shi, H.; Ren, F.; Chen, D.; Chen, Y.; Duan, Z. Augmenter of liver regeneration protects against carbon tetrachloride-induced liver injury by promoting autophagy in mice. *Oncotarget* **2017**, *8* (8), 12637−12648.
(57) Wang, M.; Zhu, C.-q.; Zeng, L.; Cheng, L.; Ma, L.; Zhang, M.; et al. Melatonin regulates the cross-talk between autophagy and apoptosis by SIRT3 in testicular Leydig cells. *Biochem. Biophys. Res. Commun.* **2021**, *555*, 182−189.
(58) Wang, M.; Wang, X.-f.; Li, Y.-m.; Chen, N.; Fan, Y.; Huang, W.-k. Cross-talk between autophagy and apoptosis regulates testicular injury/recovery induced by cadmium via PI3K with mTOR-independent pathway. *Cell Death Dis* **2020**, *11* (1), 46.
(59) Sun, M.; Hou, L.; Song, H.; Lyu, C.; Tang, Y.-d.; Qin, L. The relationship between autophagy and apoptosis during pseudorabies virus infection. *Frontiers in Veterinary Science* **2022**, *9*, 1064433.
(60) Alam, M.; Alam, S.; Shamsi, A.; Adnan, M.; Elasbali, A. M.; Al-Soud, W. A. Bax/Bcl-2 Cascade Is Regulated by the EGFR Pathway: Therapeutic Targeting of Non-Small Cell Lung Cancer. *Front Oncol* **2022**, *12*, 869672.
(61) Zhang, L.-M.; Lv, S.-S.; Fu, S.-R.; Wang, J.-Q.; Liang, L.-Y.; Li, R.-Q. Procyanidins inhibit fine particulate matter-induced vascular smooth muscle cells apoptosis via the activation of the Nrf2 signaling pathway. *Ecotoxicol Environ. Saf* **2021**, *223*, 112586.
(62) Zhu, T.; Zhang, H.; Li, S.; Wu, K.; Yin, Y.; Zhang, X. Detoxified pneumolysin derivative ΔA146Ply inhibits autophagy and induces apoptosis in acute myeloid leukemia cells by activating mTOR signaling. *Exp Mol. Med.* **2022**, *54* (5), 601−612.
(63) Qiu, Y.-N.; Wang, G.-H.; Zhou, F.; Hao, J.-J.; Tian, L.; Guan, L.-F.; et al. PM2.5 induces liver fibrosis via triggering ROS-mediated mitophagy. *Ecotoxicol Environ. Saf* **2019**, *167*, 178−187.
(64) Ryter, S. W.; Rosas, I. O.; Owen, C. A.; Martinez, F. J.; Choi, M. E.; Lee, C. G.; et al. Mitochondrial Dysfunction as a Pathogenic Mediator of Chronic Obstructive Pulmonary Disease and Idiopathic Pulmonary Fibrosis. *Annals of the American Thoracic Society* **2018**, *15* (Supplement_4), S266−S272.
(65) Ning, R.; Shi, Y.; Jiang, J.; Liang, S.; Xu, Q.; Duan, J. Mitochondrial dysfunction drives persistent vascular fibrosis in rats after short-term exposure of PM2.5. *Sci. Total Environ.* **2020**, *733*, 139135.
(66) Mizushima, N.; Levine, B.; Cuervo, A. M.; Klionsky, D. J. Autophagy fights disease through cellular self-digestion. *Nature* **2008**, *451* (7182), 1069−1075.
(67) Zhong, Y.; Xia, S.; Wang, G.; Liu, Q.; Ma, F.; Yu, Y. The interplay between mitophagy and mitochondrial ROS in acute lung injury. *Mitochondrion* **2024**, *78*, 101920.

https://doi.org/10.1021/envhealth.4c00200
Environ. Health 2025, 3, 469−481